Excitation of a slow wave structure

Peng Zhang,[1] Brad Hoff,[2] Y. Y. Lau,[1] D. M. French,[2] and J. W. Luginsland[3]
[1]*Department of Nuclear Engineering and Radiological Sciences, University of Michigan, Ann Arbor, Michigan 48109-2104, USA*
[2]*Air Force Research Laboratory, Kirtland AFB, Albuquerque, New Mexico 87117, USA*
[3]*Air Force Office of Scientific Research, Arlington, Virginia 22203, USA*

(Received 21 August 2012; accepted 27 November 2012; published online 18 December 2012)

The Green's function on a slow wave structure is constructed. The Green's function includes all radial modes, and for each radial mode, all space harmonics. We compare the analytic solution of the frequency response on the slow wave structure with that obtained from a particle-in-cell code. Favorable comparison is obtained when the first few lower order modes are resonantly excited. This gives some confidence in the prediction of converting a pulse train into radiation using a slow wave structure. © *2012 American Institute of Physics*. [http://dx.doi.org/10.1063/1.4771678]

I. INTRODUCTION

High power RF radiation sources, whether narrow-band or wide-band, typically require an electron beam. There are substantial advantages if the radiation can be generated without using an electron beam. Radiation generated using a nonlinear transmission line (NLTL) is one such approach.[1–4] The key question on this type of beam-free radiation source is the conversion of the NLTL's output voltage pulses into radiation. This paper addresses one aspect of this problem.

One way in which voltage pulses may be converted into radiation is if they are designed to excite a slow wave structure (SWS).[5] SWS readily converts an input voltage pulse into radiation when a circuit mode is excited. An example is the traveling wave tube (TWT).[6] An external AC excitation coupled to the slow wave structure would generate an electromagnetic wave or set of waves on the circuit, which could then be coupled out as radiation. For a general temporal excitation, the Green's function for the SWS is of fundamental interest.

In this paper, we shall not consider the explicit coupling of the NLTL and the SWS. Instead, we consider how the SWS would respond to an impulse excitation by constructing the Green's function. We also study the frequency response using particle-in-cell simulation on a textbook example of SWS. This textbook example of SWS[7] serves to illustrate the analytic theory and to show the structure of the Green's function for a practical SWS geometry in general. Section II describes the analytic formulation of the Green's function and the frequency response. In Sec. III, we compare the analytic formulation with the numerical code. Concluding remarks are given in Sec. IV.

II. ANALYTIC THEORY

The model of the SWS is shown in Fig. 1. It has a periodicity L in the y-direction, the vanes are infinitesimally thin,[7] and the other geometrical dimensions are specified in Fig. 1. We shall consider the excitation of two-dimensional (2D) transverse magnetic waves whose nonzero components are E_x, E_y, and H_z. To compare the analytic theory with particle-in-cell simulation, we shall assume that this slow wave structure is excited by a current source with only a J_y component. The exact relation, $\nabla^2\mathbf{H} - (1/c^2)\partial^2\mathbf{H}/\partial t^2 = -\nabla\times\mathbf{J}$, which is derived from the Maxwell equations, in frequency domain reads[8]

$$\nabla^2 H_z(x,y) + \frac{\omega^2}{c^2}H_z(x,y) = -\frac{\partial J_y(x,y)}{\partial x}. \tag{1}$$

We are in particular interested in the excitation of the SWS by a propagating ideal current sheet

$$J_y(x,y,t) = K\delta(x-a)e^{j\omega t - j\beta y}, \tag{2}$$

where K, a, ω and β are constants and δ is the Dirac delta function, and $0<a<b$ (Fig. 1). The Green's function is the SWS's response to the impulse current excitation, applied instantaneously at $(x, y, t) = (a, a', 0)$

$$\begin{aligned}\mathbf{J}(\mathbf{x},t) &= \hat{y}K\delta(x-a)\delta(y-a')\delta(t)\\ &= \hat{y}\int d\beta\int d\omega K\delta(x-a)e^{j\omega t - j\beta(y-a')}.\end{aligned} \tag{3}$$

Comparing Eq. (3) with Eq. (2), we see that the Green's function is simply the superposition, over all ω and β, of the solution to Eq. (1) subject to the plane wave excitation, Eq. (2).

The frequency domain solution to Eqs. (1) and (2) may be expressed in terms of the vacuum eigenmode solution of the slow wave structure as[8]

$$H_z(x,y) = \sum_{m=1}^{\infty} c_m H_{zm}(x,y) \equiv \sum_{m=1}^{\infty}\frac{A_m}{\omega^2-\omega_m^2}H_{zm}(x,y), \tag{4}$$

where the mth eigenfunction, H_{zm}, with the eigenfrequency ω_m at the specified value of β satisfies the vacuum eigenmode equation

$$\nabla^2 H_{zm}(x,y) + \frac{\omega_m^2}{c^2}H_{zm}(x,y) = 0. \tag{5}$$

In writing the last form of Eq. (4), we explicitly show an infinite response if the SWS, which is assumed to be lossless, is

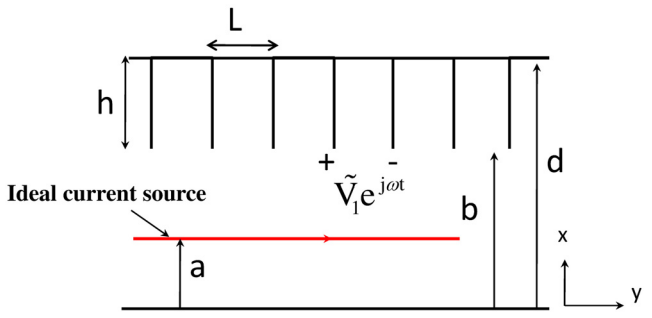

FIG. 1. Slow wave structure, excited by an ideal current source.

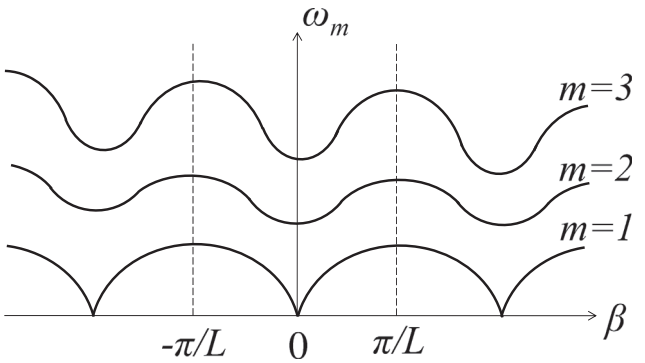

FIG. 2. Schematic drawing of the cold-tube dispersion relation $\omega_m(\beta)$. The lowest three radial modes are shown.

resonantly excited at the frequency $\omega = \omega_m$ (see Fig. 3 below).

The Green's function $G(x,y,t)$, which is the solution H_z in the SWS in response to the impulse current excitation, Eq. (3), then reads

$$G(x,y,t) = \int d\beta \int d\omega e^{j\omega t - j\beta(y-a')} \sum_{m=1}^{\infty} c_m H_{zm}(x,y). \quad (6)$$

We show in Appendix that Eq. (6) may be written in the general form

$$G(x,y,t) = \sum_{m=1}^{\infty} \sum_{l=-\infty}^{\infty} \int_0^{2\pi/L} d\beta e^{-j(\beta+2\pi l L)(y-a')} \times \frac{2\pi \sin(\omega_m t)}{\omega_m} A_m H_{zm}(x,y), \quad (7)$$

where A_m is defined in Eq. (4). The contribution from each radial mode (m), and from each space harmonic (ℓ), to the Green's function is apparent in Eq. (7); it can also be calculated numerically. Note the general form of the Green's function, as displayed in Eq. (7), for a periodic SWS.

For the geometry of Fig. 1, $\omega_m = \omega_m(\beta)$ is the mth root to $D(\omega,\beta) = 0$, where[7,8]

$$D(\omega,\beta) \equiv \frac{\cot(\omega h/c)}{\omega h/c} - \sum_{n=-\infty}^{\infty} \left(\frac{\sin\theta_n}{\theta_n}\right)^2 \frac{\coth(\gamma_n b)}{\gamma_n h} \quad (8)$$

and θ_n and γ_n are defined as

$$\begin{aligned} \theta_n &= \beta_n L/2, & n &= 0, \pm 1, \pm 2, \ldots \\ \gamma_n &= \sqrt{\beta_n^2 - \frac{\omega^2}{c^2}}, & n &= 0, \pm 1, \pm 2, \ldots \\ \beta_n &= \beta + 2n\pi/L, & n &= 0, \pm 1, \pm 2, \ldots \end{aligned} \quad (9)$$

The cold tube dispersion relation $\omega_m(\beta)$ is schematically shown in Fig. 2, which shows the first three "radial" modes $m = 1$, 2, and 3 where m designates the mode number in the x-direction in Fig. 1. These vacuum modes were studied in detail in Ref. 8 and will not be repeated here. We follow Ref. 8 to normalize the vacuum eigenmode according to $\int\int dxdy|H_{zm}(x,y)|^2 = 1$, where the double integral is carried over one period of the SWS shown in Fig. 1. For the ideal current source given by Eq. (2), the complex amplitude, c_m in Eq. (4), of the mth excited mode reads

$$\begin{aligned} c_m &\equiv \frac{A_m}{\omega^2 - \omega_m^2} \\ &= \frac{-j\omega_m \varepsilon_0 c^2}{\omega^2 - \omega_m^2} (KL) d_m \left[\frac{\sinh(\gamma_{m0} a)}{\sinh(\gamma_{m0} b)}\right] \sin\left(\frac{\omega_m h}{c}\right) \frac{\sin(\beta L/2)}{\beta L/2}, \end{aligned} \quad (10)$$

$$d_m = \frac{1}{\sqrt{L\left(\frac{\varepsilon_0}{\mu_0}\right)(h_m + f_m)}}, \quad (11)$$

$$h_m = \int_b^d dx \cos^2\left[\frac{\omega_m(x-d)}{c}\right], \quad (12)$$

$$f_m = \sum_{n=-\infty}^{\infty} \frac{\omega_m^2}{c^2|\gamma_{mn}^2|} g_{mn} \frac{\sin^2(\omega_m h/c)}{|\sinh(\gamma_{mn} b)|^2} \left[\frac{\sin(\beta_n L/2)}{\beta_n L/2}\right]^2, \quad (13)$$

$$g_{mn} = \int_0^b dx |\cosh^2(\gamma_{mn} x)|, \quad (14)$$

$$\gamma_{mn} = \sqrt{\beta_n^2 - \frac{\omega_m^2}{c^2}}, \quad n = 0, \pm 1, \pm 2, \ldots \cdot \quad (15)$$

Since the Green's function, Eq. (7), depends on all modes and is valid for arbitrary (x,y,t), its benchmark against numerical codes is infeasible. Thus, we resort to comparing the crucial components that form the building block of the Green's function. Specifically, we calculate the frequency response, $\tilde{V}_1(\omega)$, of the voltage across a pair of vane tips when the excitation current is given by Eq. (2) with a pre-assigned value β. With the tip voltage written as $V_1(t) = \tilde{V}_1(\omega)e^{j\omega t}$, (Fig. 1) we find

$$\tilde{V}_1(\omega) = -L \sum_{m=1}^{\infty} \left(\frac{\omega_m}{\omega}\right) c_m d_m \sin\left(\frac{\omega_m h}{c}\right), \quad (16)$$

to within a constant phase factor by the Floquet Theorem.[7] The frequency response $\tilde{V}_1$ as a function of ω is plotted in Fig. 3 for the following parameters: $b/L = 6.0$, $h/L = 6.0$, $a/L = 5.8$, $\beta L = \pi/2$. The divergence of $\tilde{V}_1$ shown in Fig. 3 occurs at $\omega = \omega_m$, at which c_m is singular in Eq. (10).

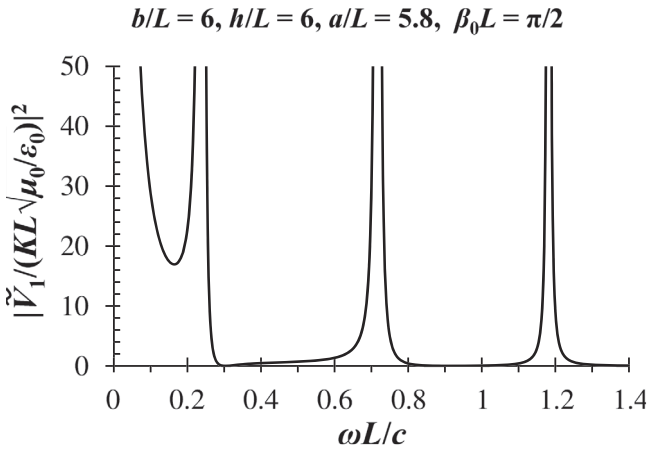

FIG. 3. The frequency response $\tilde{V}_1$ as a function of $\omega L/c$ for the following parameters: $b/L = 6.0$, $h/L = 6.0$, $a/L = 5.8$, $\beta_0 L = \pi/2$.

Since the model so far is lossless, the frequency response $\tilde{V}_1$ is infinite when the drive frequency coincides with a resonant frequency, $\omega = \omega_m$. The structure would have a finite response at the resonant frequency by including a finite quality factor, Q. The effect of a finite Q may be modeled by replacing the resonant factor $(\omega^2 - \omega_m^2)$ in c_m with $(\omega^2 - j\omega\omega_m/Q_m - \omega_m^2)$, where Q_m represents the quality factor of the mth eigenmode.[7] We shall use this technique to compare the analytic results with the numerical simulation, which is described next.

III. PARTICLE-IN-CELL SIMULATION

In this section, we use the ICEPIC particle-in-cell code[9] to simulate the response of the slow wave structure and compare with the analytic theory.

Simulations were performed in 2-D geometry, shown in Fig. 4. The third dimension, Z, is ignored. Two artificially heavy particle beams ($|e/m| = 1.602 \times 10^{-9}$ C/kg) are launched from the emitter on the left-hand side of the simulation. The beams travel toward the collector on the right-hand side of the simulation, where they are absorbed. The first beam is a constant-amplitude beam of "positrons" with $K = 1$, in A/m. The second beam is a charge modulated "electron" beam with $K = -1 - \sin[(c/L)*(\omega L/c)*t]$, also in A/m. The velocity of both beams is selected to be $(c/\beta L)*(\omega L/c)$. The combination of the two beams yields an effective current sheet with the spatial and temporal modulations corresponding to the $(\omega L/c)$ and (βL) values chosen [cf. Eq. (2)].

Resolution was set at 5 mm for both X and Y grids. The period length, L, was defined to be 10 cm. The remaining geometry was then constrained per the ratios given in the caption of Fig. 3. The slow wave structure consisted of a constant height section (200 periods in length), with tapered sections (50 periods) at either end. All slow wave structure vanes were one cell thick in the Y direction, making the cavity widths 9.5 cm.

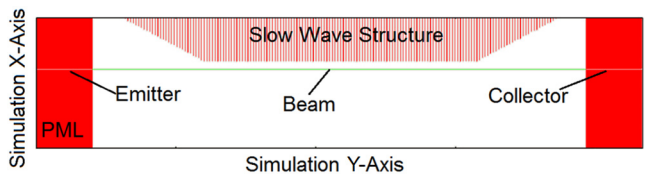

FIG. 4. Simulation geometry.

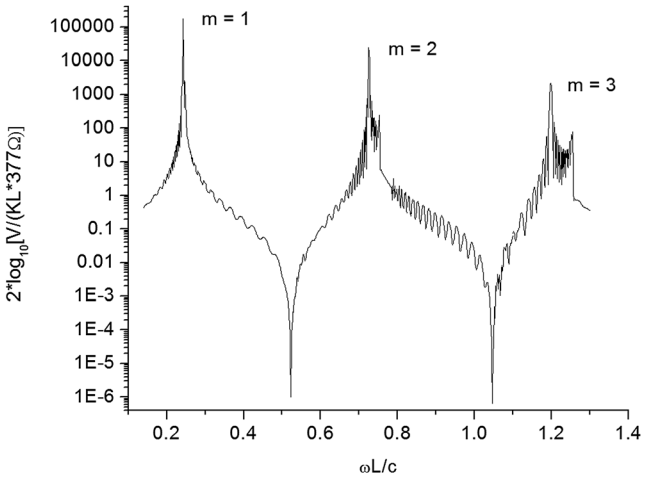

FIG. 5. Normalized simulation amplitude data for $\omega L/c$ values of 0.140 to 1.300. The $m = 1$, 2, and 3 peaks are depicted (with the $m = 1$ peak being the leftmost peak).

The tapered slow wave structure sections were separated from regions of perfectly matched load (PML,[10] 20 periods in length) by vacuum sections 15 periods in length. The emitter and collector, which pass through the PML regions, were one cell thick in the X direction and 20 periods long. The inter-vane voltage measurement was made using an $E \bullet dl$ line integral extending from the tip of vane 100 to the tip of vane 101 of the center section of the slow wave structure.

Data for $\omega L/c$ values ranging from 0.140 to 1.300 are plotted in Fig. 5. Due to the wide range in peak heights, the base 10 log is taken of the normalized amplitude scale described previously in Fig. 3. The leftmost peak in Fig. 3 corresponds to the intersection with the $m = 1$ branch of the dispersion relation qualitatively depicted in Fig. 2, with the $m = 2$ and $m = 3$ peaks following sequentially to the right. The peak locations in the ICEPIC simulations were found to occur within 1.5% of the analytically predicted values. A pseudocolor plot of the Y component of the electric field is provided in Fig. 6. Figures 6(a)–6(c) correspond to the $m = 1$, 2, and 3 peaks of Fig. 5,

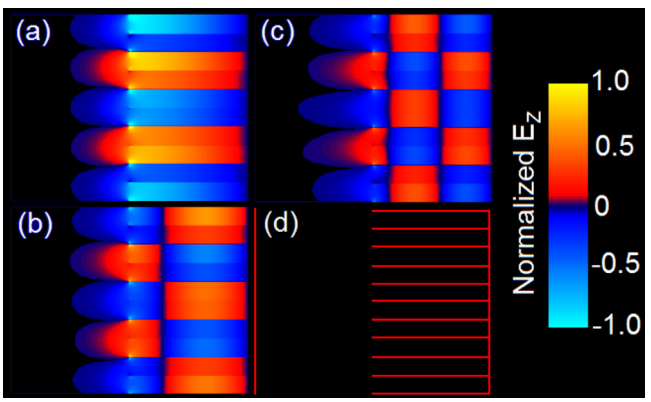

FIG. 6. Pseudocolor plot of the Y component of the electric field. Plots corresponding to the $m = 1$ (a), $m = 2$ (b), and $m = 3$ (c) mode. Peaks are provided along with a grid plot of the simulated slow wave structure (d). Scale multipliers for (a), (b), and (c) are 1×10^5 V/m, 5×10^4 V/m, and 4×10^4 V/m, respectively.

respectively. For reference, a grid plot showing the slow wave structure is depicted in Fig. 6(d).

It is well known that the Q of a system can be represented by the total energy present in a system divided by the total energy lost from the system over one RF cycle. For the arrangement considered by the analytic calculations, infinitely high Q values are possible as no energy leaves the system. As previously described, the ICEPIC simulations presented here utilize a finite slow wave structure terminated on either end with tapered sections and perfectly matched load regions. The presence of these load regions represents an energy loss mechanism within the simulation space. This energy loss will necessarily result in finite Q values and thus finite width resonance peaks.

The comparison between the ICEPIC simulations and the analytic theory follows. First, to make the analytic frequency response finite at $\omega = \omega_m$ in Eq. (10), we introduce a finite quality factor Q_m in the manner given in the last paragraph of Sec. II. The value of Q_m is adjusted so that the resonant peak at $\omega = \omega_{\mathrm{m}}$ is the same between the analytic theory and the simulation, as shown in Fig. 7. The introduction of such a phenomenological Q_m is necessary because of the very different approximations that have been made between the analytic model and the simulation, all of which might affect the value of Q for *each* radial mode. Note that in the analytic theory, fixing the value of Q_m would also fix the linewidth at $\omega = \omega_m$, in addition to the peak voltage at the vane tip. From Fig. 7, we see that the values of such a composite "loaded Q" are quite reasonable, for both the analytical and simulation model.

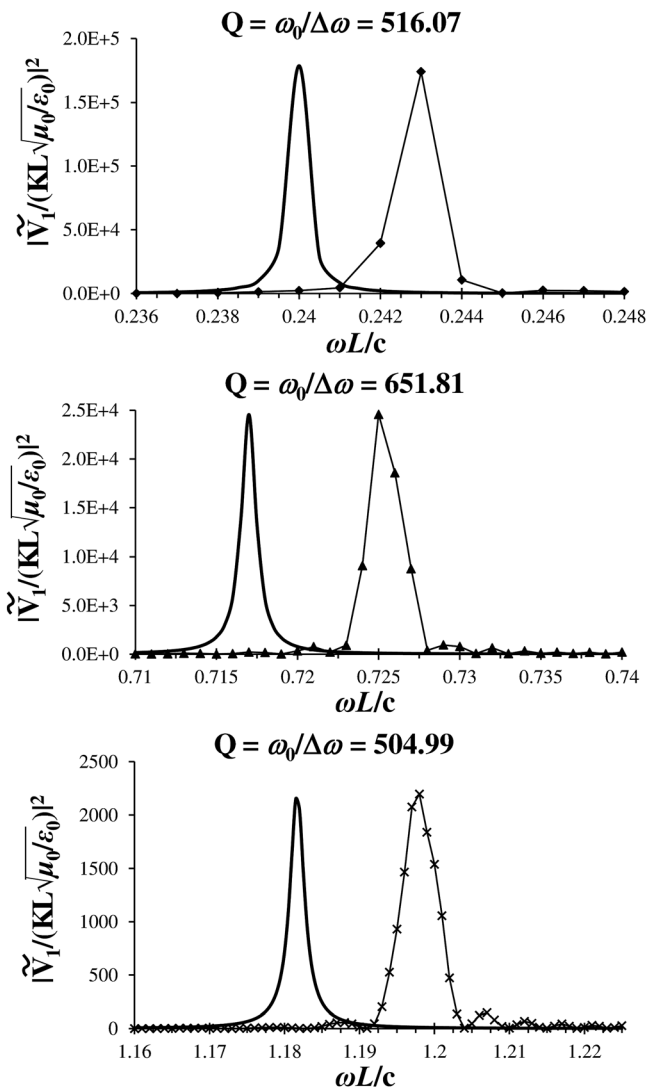

FIG. 7. Comparison of the frequency response in the analytic theory (left curves) and ICEPIC simulation (right curves), for the $m = 1$, 2, and 3 modes (top to bottom). The values of Q are chosen so that the peak response in the analytic theory matches that of the ICEPIC simulation for each m-mode.

IV. CONCLUDING REMARKS

The excitation of a slow wave structure by a series of impulses has been determined analytically by developing the Green's function for the system which includes all spatial harmonics and all radial modes. Since any signal can be represented by a superposition of impulses, the solution derived here can be used to determine the excitation of a SWS driven by an arbitrary temporal signal. The analytic solution was compared to particle-in-cell calculations in which an ideal current excitation is used to measure the response of the SWS. A finite Q was introduced into the analytical solution to account for previously mentioned effects which result in a finite line width in the simulations. Despite the differences in the geometry and in the approximations made between the analytic and simulation models, the resonant peak locations ($\omega L/c$ values) in the ICEPIC simulations were found to agree with analytically predicted values to within 1.5%. The ability to analytically predict excitation of RF within pulse excited systems not only furnishes a vital tool to guide experimental efforts but also provides capabilities to benchmark computational algorithm development.

ACKNOWLEDGMENTS

The authors would like to acknowledge helpful discussions with P. J. Mardahl of the Air Force Research Laboratory regarding the ICEPIC code. This work was supported by the Air Force Office of Scientific Research Award FA9550-09-1-0662, AFOSR LRIR 12RD02COR, and by the Department of Defense High Performance Computer Modernization Program under subproject AFKED01314C4O.

APPENDIX: THE GREENS' FUNCTION

This appendix presents a form of the Green's function which may be computed numerically. It also displays the contributions to the Green's function from the various radial modes and their space harmonics. The generality of the structure of the Green's function is noted.

Equation (6) may be rewritten as

$$G(x,y,t) = \sum_{m=1}^{\infty} \int d\beta e^{-j\beta(y-a')} \int d\omega e^{j\omega t} c_m H_{zm}(x,y)$$
$$= \sum_{m=1}^{\infty} \int_{-\infty}^{\infty} d\beta e^{-j\beta(y-a')} A_m H_{zm}(x,y) \int_{\Gamma} d\omega \frac{e^{j\omega t}}{\omega^2 - \omega_m^2}, \tag{A1}$$

where we have used Eq. (4) and the fact that A_m and $H_{zm}(x,y)$ are independent of ω. In the last integral of Eq. (A1), the contour Γ lies in the lower half complex ω-plane, according to the Laplace transform theory.[11] Since $\omega_m = \omega_m(\beta)$ is real for real β (Fig. 2), the simple residue theory yields[11]

$$\int_{-\infty}^{\infty} d\omega \frac{e^{j\omega t}}{\omega^2 - \omega_m^2} = \frac{2\pi}{\omega_m}\sin(\omega_m t), \quad t > 0. \tag{A2}$$

Inserting Eq. (A2) into Eq. (A1), we obtain

$$G(x,y,t) = \sum_{m=1}^{\infty} \int_{-\infty}^{\infty} d\beta e^{-j\beta(y-a')} F(\beta), \tag{A3}$$

$$F(\beta) = \frac{2\pi\sin(\omega_m t)}{\omega_m} A_m H_{zm}(x,y). \tag{A4}$$

From Bloch's theorem,[7] both ω_m and $F(\beta)$ are periodic in β with period $2\pi/L$. The integral in Eq. (A3) may then be further simplified

$$\int_{-\infty}^{\infty} d\beta e^{-j\beta(y-a')} F(\beta) = \sum_{l=-\infty}^{\infty} \int_{2\pi l/L}^{2\pi(l+1)/L} d\beta e^{-j\beta(y-a')} F(\beta)$$
$$= \sum_{l=-\infty}^{\infty} \int_{0}^{2\pi/L} d\beta' e^{-j(\beta'+2\pi lL)(y-a')} F(\beta'+2\pi l/L), \tag{A5}$$

where $\beta' = \beta - 2\pi l/L$. We may now drop the prime in the dummy variable β' in the last of Eq. (A5). Equations (A3)–(A5) then give

$$G(x,y,t) = \sum_{m=1}^{\infty}\sum_{l=-\infty}^{\infty} \int_{0}^{2\pi/L} d\beta e^{-j(\beta+2\pi lL)(y-a')} \times \frac{2\pi\sin(\omega_m t)}{\omega_m} A_m H_{zm}(x,y), \tag{A6}$$

which can be calculated numerically. Physically, Eq. (A6) explicitly gives the contribution to the Green's function from each space harmonics (ℓ) of every radial mode (m). Comparing Eq. (A6) with Eq. (4) of the main text, we note the generality of the Green's function (A6) for a periodic slow wave structure.

[1] A. M. Belyantsev, A. I. Dubnev, S. L. Climin, Yu A. Kobelev, and L. A. Ostrovsky, "Generation of radiopulses by EMSW on ferrite transmission lines," Zh. Tekh. Fiz. **65**(8), 132–142 (1995).
[2] N. Seddon, C. Spikings, and J. Dolan, "RF pulse formation in nonlinear transmission lines," in *2007 16th IEEE International Pulsed Power Conference*, *Albuquerque, New Mexico, USA* (2007), Vol. 1, pp. 678–681.
[3] J. Darling and P. Smith, "High-power pulsed RF extraction from nonlinear lumped element transmission lines," IEEE Trans. Plasma Sci. **36**, 2598–2603 (2008).
[4] Q. R. Marksteiner, B. Carlsten, and S. Russell, "Efficient generation of RF using a biased soliton generating nonlinear transmission line with a bipolar input," Microwave Opt. Technol. Lett. **52**, 1411–1413 (2010).
[5] B. W. Hoff, D. M. French, S. L. Heidger, and A. D. Greenwood, "Nonlinear transmission line extraction systems," U.S. patent filing 13/469,005 (2012).
[6] R. J. Barker, J. H. Booske, N. C. Luhmann, and G. S. Nusinovich, *Modern Microwave and Millimeter Wave Power Electronics* (IEEE, Piscataway, NJ, 2005).
[7] J. W. Gewartowski and H. A. Watson, *Principles of Electron Tubes* (Van Norstrand, New York, 1965).
[8] Y. Y. Lau and D. Chernin, Phys. Fluids **B 4**, 3473 (1992).
[9] R. J. Peterkin and J. W. Luginsland, "A virtual prototyping environment for directed-energy concepts," Comput. Sci. Eng. **4**(2), 42–49 (2002).
[10] B. Jean-Pierre, "A perfectly matched layer for the absorption of electromagnetic waves," J. Comput. Phys. **114**(2), 185–200 (1994).
[11] F. B. Hilderbrand, *Advanced Calculus for Applications* (Prentice-Hall, Englewood, Cliffs, NJ, 1962).